# Femtosecond laser pulse splitting effect in second harmonic generation under Laue diffraction in one-dimensional photonic crystals

V. B. Novikov * and T. V. Murzina
*Department of Physics, M. V. Lomonosov Moscow State University, Moscow 119991, Russia*

(Received 22 December 2020; revised 25 May 2021; accepted 26 May 2021; published 4 June 2021)

The ability to manipulate the frequency of light is a cornerstone of a wide range of applications in photonics expanding spectral ranges of the light sources. To boost the second harmonic generation efficiency, intense efforts toward exploiting artificial microstructures for frequency doubling were carried out. The sought-after approach of utilizing photonic crystals is inspired by their unusual light dispersion. In such structures, the dynamics of the field of femtosecond laser pulses is of paramount importance for frequency conversion. In this work, we investigate the phase-matched second harmonic generation under the effect of diffraction-induced femtosecond laser pulse splitting in one-dimensional photonic crystals at the Bragg diffraction in the Laue geometry. We demonstrate that the interaction of the two pulses at the fundamental frequency that appears in photonic crystals through the dynamical light diffraction leads to a nonmonotonic dependence of the frequency up-conversion efficiency with respect to the laser pulse duration, thus allowing to increase the second harmonic power by tuning the pulse duration.

DOI: 10.1103/PhysRevB.103.235408

## I. INTRODUCTION

Nonlinear optical processes of frequency conversion are of practical interest in creating new coherent light sources. It allows one to extend the spectral ranges of available laser systems, which is important both in a research and industry [1]. Optical second harmonic generation (SHG) that is the process of the frequency doubling of the laser radiation in a nonlinear medium is the basic nonlinear optical effect. Recent decades have witnessed intense efforts toward exploiting artificial optical microstructures to increase the SHG efficiency. Judiciously designed, they can benefit in the enhancement of the SHG due to resonant localization of the electromagnetic field and fulfillment of the phase-matching conditions [2–4].

In the begining, metal nanostructures marveled for their plasmonic resonances and electromagnetic field localization were used to intensify the SHG [5] by excitation of the localized plasmons in isolated nanoparticles [6], plasmonic nanoantenna [7], surface plasmon-polaritons in plasmonic crystals [8], and even hybrid plasmonic-photonic structures [9]. To overcome the drawback of optical losses in metals, it was suggested recently to use nonlinear metasurfaces, which can boost the frequency conversion due to the Mie resonances [10–13] and bound states in the continuum [14]. In spite of the achieved record up-conversion efficiency of microstructures it remains smaller compared to the SHG in extended nonlinear crystals. In the latter ones, the fulfillment of the phase- and quasi-phase-matching conditions is the main desired effect instead of the field enhancement.

Periodically poled nonlinear crystals with spatial periodicity of the second-order nonlinear susceptibility and homogeneous refractive index allow one to overcome this roadblock due to the nonlinear diffraction [15–17]. On the other hand, photonic crystals (PhCs) with spatial periodicity of the refractive index are considered as a fertile platform for the SHG. The phase-matched SHG in layered PhC waveguides was achieved when exploiting the form birefringence of artificial stack of the subwavelength-thick dielectric layers [18,19]. When the PhC period is comparable to the wavelength of light, phase- and quasiphase-matching can be achieved at the photonic band gap (PBG) edge due to strong lattice-induced light dispersion [20–25]. A promising approach for the versatile light manipulation based on the Laue diffraction in diffraction-thick 1D layered PhCs was proposed very recently [26–36]. For example, the pendulum effect [26–28] was suggested for light switching. Under the Laue diffraction periodical losses in 1D PhC lead to the anomalous high transmission of light or the Borrmann effect [29], which can be intensified by the topological transition [30] and is useful for spatial beam filtering. The existence of the Laue soliton was predicted for a PhC containing resonant two-level atoms, which can be considered as a nonlinear analog of the Borrmann effect [31]. Combination of loss and gain regions in the parity-time symmetric 1D PhCs leads to asymmetric pendulum effect and unidirectional pulse-splitting at the Laue diffraction [32–34]. As well the Laue diffraction serves for the phase- and quasi-phase-matched second harmonic generation [35,36].

The nonlinear origin of the SHG process requires the usage of femto- or picosecond pulsed fundamental radiation with high peak field amplitude. This requirement makes the field dynamics imperative for the effective SHG in extended structures with the length considerably exceeding the pulse width. It has found a tremendous success in PhCs with unusually strong dispersion and inspired the slow light effect in PhC

*vb.novikov@physics.msu.ru

 

waveguides for brilliant frequency conversion [37]. Recently, the approach of the intermodal nonlinear interaction in multimode waveguides and photonic crystals fibers have attracted much attention in four-wave-mixing [38–40], biphoton generation [41], stimulated Raman scattering [42]. The involvement of several different guided modes of the pump radiation affords new degrees of freedom for the phase-matching that was exploited for highly tunable frequency conversion [39,40]. Promising approach of intermode interaction requires to treat the group-velocity mismatch when femtosecond laser pulses are applied [43]. Interaction of ultrashort laser pulses with PhCs could be accompanied by pronounced pulse dynamics. The dynamical Bragg diffraction of light in 1D PhC in the Laue geometry leads to the pulse-splitting effect consisting of splitting of a single incident femtosecond pulse in a PhC to the pair of pulses with different group velocities [28,44]. We assert that this effect should influence the second harmonic (SH) response of PhCs. To the best of our knowledge, this effect has not been considered in the nonlinear optics of the PhCs. We suppose that provided here insight and experimental results could be extended to intermode nonlinear optical interaction in waveguides and photonic crystal fibers and could be useful for understanding of other nonlinear effects like intermodal four-wave-mixing when ultrashort laser pulses are involved.

In this work, we study the phase-matched SHG in 1D PhC under the Bragg diffraction in the Laue geometry in the presence of the laser pulse-splitting effect. By meticulous constructing of the PhC, we achieve the phase-matched SHG induced by the interaction of the two laser pulses appearing due to the pulse splitting effect. We prove experimentally the decisive role of the femtosecond laser pulse splitting in a PhC in the SHG process, and further elucidate the fundamental aspects of SHG by numerical simulations. The paper is organized as follows. In Sec. II, we give the details of the sample preparation and carried out experiments. Then in Sec. III, we present and discuss the choice of the PhC' parameters for the phase-matched SHG, splitting of the fundamental radiation pulse and results of numerical simulation of SHG, followed by Conclusion.

## II. EXPERIMENT DETAILS

The 1D PhC was obtained by electrochemical etching [45,46] of the silicon wafer followed by full thermal annealing that results in the composition of lossless porous silica PhC. Briefly, in this procedure electrochemical cell with a tungsten spiral wire cathode and a crystalline silicon wafer anode was used. We etched p + + boron-doped silicon wafer with (001) orientation and resistance of $\rho = 0.005\ \Omega\,\mathrm{cm}$. The application of dc current with alternating in time densities of $j_1 = 200\ \mathrm{mA/cm^2}$ and $j_2 = 40\ \mathrm{mA/cm^2}$ formed the PhC with a two-layered unit cell in the direction along the normal to the wafer. Each nanoporous PhC layer with the pores' diameter of about several tens of nanometers can be characterized by effective refractive index. The porosity ($p$) as well as the refractive index ($n$) of the layers alternated and took the values of $p_1 = 0.73$, $n_1(800\ \mathrm{nm}) = 1.50 + i0.8 \times 10^{-3}$ for the first layer and $p_2 = 0.57$, $n_2(800\ \mathrm{nm}) = 2.00 + i2.2 \times 10^{-3}$ for the second layer in the unit cell. Then thermal annealing of the structure was performed at 650 °C at ambient atmosphere

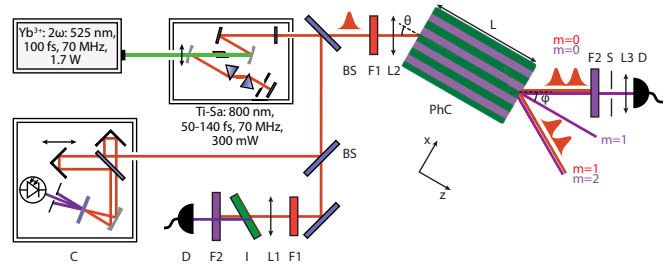


FIG. 1. Scheme of the experimental setup. Elements: C: autocorrelator, BS: beam splitter, L1, L2, L3: lenses, I: ITO film, F1: filter RG-695, F2: filter BG-39, D: photomultiplier tube, S: slit aperture, and PhC: photonic crystal. Diffraction orders $m$ of the fundamental and SH light are shown by red and violet, correspondingly.

to obtain the PhC transparent in visible spectral range. Second order nonlinear susceptibility was introduced by the PhC's pore infiltration by the water solution of a ferroelectric salt (sodium nitrite) followed by slow evaporation as described in Ref. [35]. Incorporation of the ferroelectric increased refractive indices of porous silica layers by approximately $10^{-3}$. The final PhC consisted of 870 layers with the refractive indexes of $n_1(800\ \mathrm{nm}) = 1.105$, $n_1(400\ \mathrm{nm}) = 1.11$ and $n_2(800\ \mathrm{nm}) = 1.21$, $n_2(400\ \mathrm{nm}) = 1.22$ and the thicknesses of $d_1 = 590$ nm, $d_2 = 315$ nm. These parameters of the PhC corresponded to the SHG phase-matching condition as described below in Sec. III. The PhC was wedge-shaped in the (YOZ)-plane allowing us to vary its length $L$ in the range of 250–500 $\mu$m (Fig. 1). The experimental SHG setup is sketched in Fig. 1. It involves a femtosecond Ti:sapphire laser with the pulse repetition rate of 70 MHz pumped by the second harmonic of another femtosecond $Yb^{3+}$ laser (TEMA-Duo, Avesta Project). The duration ($\tau$) of Ti:sapphire laser pulses could be varied in the range of 50–140 fs by changing the negative dispersion introduced by a prism compressor situated in the Ti:sapphire laser resonator and controlled by the autocorrelator (MINI, APE Angewandte Physik und Elektronik GmbH). The latter was based on the measurements of the SH intensity generated in the BBO crystal as a function of the time delay between the pulses in the two arms of the autocorrelator. To simultaneously compare the SHG in PhC and in a thin nonlinear film, the reference SH channel was used with a 30-nm-thick ITO film on a glass substrate, the SHG intensity being detected by a photomultiplier tube (R4220P, Hamamatsu) operating in the photon counting regime. In the signal channel, the fundamental beam with the central wavelength of 800 nm was focused by a lens with the focal distance of $f = 5$ cm on the PhC's facet at the Bragg angle of $\theta = 26°$. The SH signal generated in the PhC was extracted by appropriate color filters and measured by a photomultiplier as well.

At the Bragg diffraction, the incident fundamental beam refracted inside the PhC in such a way that light propagated along the PhC's layers (Fig. 1). In free space after the PhC, we observed the two fundamental diffraction beams of the zero ($m = 0$) and the first ($m = 1$) orders corresponding to the scattering angles of $\varphi = 0°$ and 52° counted from the incident beam direction as illustrated by red lines in Fig. 1. They originate from the Bragg diffraction of the laser beam in the

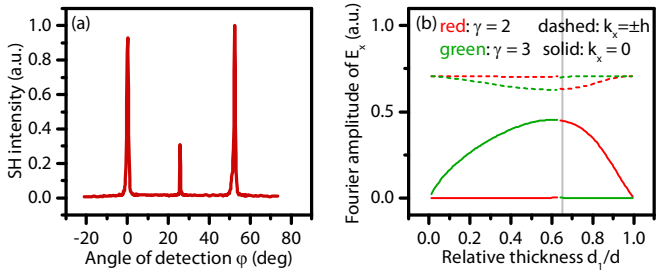


FIG. 2. (a) Measured indicatrix of the SH intensity; angle $\varphi = 0^\circ$ corresponds to the direction of transmission. (b) Calculated dependencies of the spatial Fourier components of the electric field of the two Bloch modes $\gamma = 2, 3$ of the SH radiation on the relative thickness of layers with $n_1$. Dashed curves: Fourier components for $k_x = \pm h$, solid curves: the same for $k_x = 0$. Vertical line indicates the relative layer thickness of the experimental PhC.

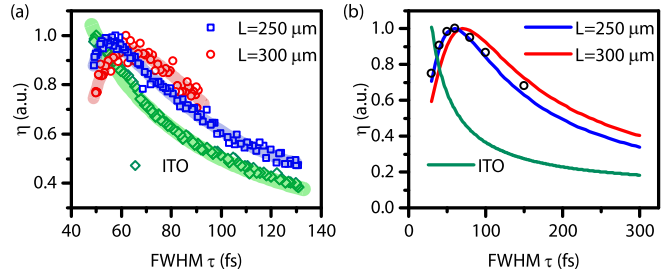


FIG. 4. (a) Experimental dependencies of the normalized SH power $\eta$ in transmitted beam on the duration of the incident pulse duration for PhCs with the length $L = 250$ $\mu$m (blue dots) and 300 $\mu$m (red dots). Green dots: SH power from ITO film. (b) The same dependence calculated in the scope of slow varying envelope approximation (solid curves). Result of the nonlinear FDTD simulation for $L = 250$ $\mu$m (dots).

PhC. At the same time we disclosed that the SH signal forms three well directed outgoing beams as demonstrated by the SH indicatrix [Fig. 2(a)] measured by the photomultiplier tube mounted on the rotation stage and supplied by a slit aperture allowing the angular resolution of 0.5°. The two side maxima of the SH indicatrix (at $\varphi = 0^\circ$ and 52°) are codirectional to the zero- and first order diffraction maxima of the fundamental radiation, while the central one is the first order-diffraction maxima for the nonlinear signal (Fig. 1). We observed that the angular divergence of the SH maxima of 0.9° is more than four times smaller than 4° divergence of the fundamental beams. High directivity of the SHG response and its disappearance at angular and spectral detuning of the fundamental incident beam confirm the phase-matched SHG in analogy with results of our foregoing work [35].

Turning to the dynamics of the light pulses in the PhC, first we assert that the considered PhC structure sustains the effect of the femtosecond pulse splitting, which appears as a couple of consecutive pulses in each diffraction maxima, as exemplified in Fig. 1. We revealed this by measuring the intensity autocorrelation function of the outgoing pump radiation for a PhC with the length of $L = 500$ $\mu$m and incident pulse width of 60 fs [Fig. 3(a)]. Assuming the Gaussian envelope of the pulses, we reconstruct the temporal dependence of the intensity of the transmitted beam, which shows that it consists

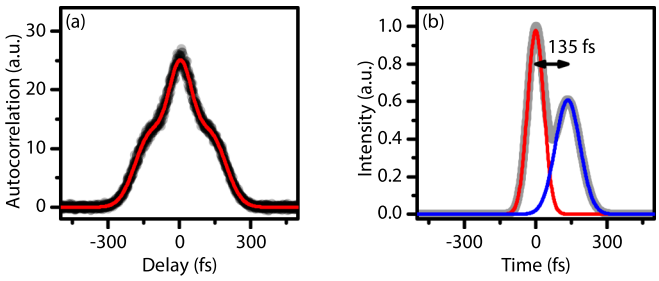


FIG. 3. (a) Measured autocorrelation function in zero-order diffraction beam. Dots: experiment, red curve: fit. (b) Reconstructed temporal dependence of the intensity of the fundamental radiation (gray curve). Red and blue curves - Gaussian fit of the two pulses.

of the two outgoing pulses with the interpulse delay of about 135 fs [Fig. 3(b)].

We harnessed the dependence of the SH power on the duration of the incident femtosecond pulses in order to investigate the effect of the pulse-splitting of the fundamental radiation on the frequency up-conversion. For this we used the SH power ($P_{2\omega}$) in the zero-order beam normalized to the incident pump power squared, ($P_\omega$), i.e., the value $\eta = P_{2\omega}/P_\omega^2$. The measured dependence of $\eta$ on the pulse duration $\tau$ (FWHM) and normalized to its maximum is shown in Fig. 4(a) and is not trivial. It demonstrates nonmonotonic dependence with the growth for the short pulses and a decrease for the long ones, and possesses the maximum at $\tau = 55 \pm 3$ fs for the PhC' length $L = 250$ $\mu$m and $\tau = 62 \pm 3$ fs for $L = 300$ $\mu$m, i.e., the maximum shifts toward larger pulse widths when the PhC length is increased. At the same time, for thin ITO film, $\eta$ decreases monotonically (inversely proportional to $\tau$). We assert that the revealed peculiarities of SHG in the PhC are the results of the pulse-splitting effect at the fundamental frequency, as will be demonstrated in the next section.

## III. THEORY AND DISCUSSION

Lattice-induced light dispersion in a PhC is a powerful platform for the elimination of the SHG phase mismatch. In order to achieve the phase-matched SHG, we applied the method proposed in Ref. [35] based on tuning of the thickness of the PhC layers. Periodical structure of the 1D PhC offers plethora of eigenmodes of light inside the PhC with different propagation constants $q_z^{(\gamma)}$. The related calculated isofrequency curves for the p-polarized fundamental and SH radiations are shown in Fig. 5(b). Eigenmodes are enumerated by the index $\gamma$ in descending order on $q_z$. The isofrequency curves of eigenmodes valuable for the phase-matched SHG are colored in Figure 5(b). The fundamental eigenmodes highlighted in Fig. 5(b) are chosen as possessing high amplitudes, and second harmonic ones that can participate in the phase-matched SHG process. When the fundamental radiation is incident at the Bragg angle, a couple of eigenmodes with $\gamma = 1, 2$ propagates in the PhC with similar amplitudes shown by blue and red curves in Fig. 5(b) and also known as the anti-Borrmann and Borrmann ones [44]. Self- or cross-interactions

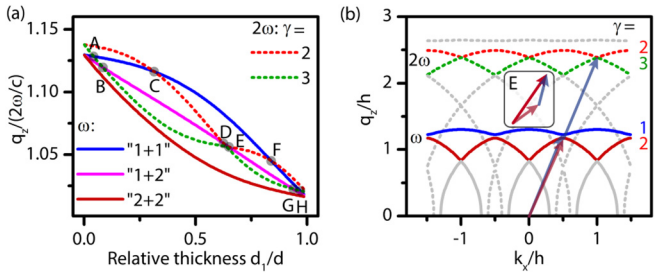


FIG. 5. (a) Propagation constants of the SH modes (solids) and nonlinear polarization waves (dashed) versus the relative thickness of the low refractive index layers. Notation "$\gamma_1 + \gamma_2$" means interaction of $\gamma_1$th and $\gamma_2$th fundamental modes. (b) Isofrequency curves for the $p$-polarized light with the wavelengths of 800 nm (solid) and 400 nm (dashed). The inset is the wave-vector diagram of the phase-matching condition denoted by letter E on the left panel.

of these modes in a second-order nonlinear process generate three waves of the nonlinear polarization with $2q_z^{(1,2)}$, $q_z^{(1)} + q_z^{(2)}$, respectively. Solid curves in Fig. 5(a) show the dependence of the propagation constants of these waves, which are normalized to the SH vacuum wavenumber, on the relative thickness of the low refractive index layers. The normalized $q_z$ for the SH eigenmodes are shown by dashed curves. The eight crossing points labeled by the letters (A-H) indicate the possible phase-matching conditions for the SHG.

Ultimately fabricated PhC structure described in Sec II corresponds to the E point, the wave-vector diagram of which is sketched in the inset of Fig. 5(b). In this case, two fundamental eigenmodes with the numbers $\gamma = 1$ and $\gamma = 2$ lead to the phase-matched excitation of the SH eigenmode with $\gamma = 2$. The cross-interaction of the fundamental eigenmodes has a primarily importance for the observed temporal dependence of the SH power as shown below.

To lift the veil on the nature of the nonmonotonic dependence of $\eta$ in considered phase-matched process, here we provide an intuitive physical picture and then supplement it by the numerical proof. When the $p$-polarized fundamental femtosecond pulse is incident at the Bragg angle, two pulses formed by the Borrmann and anti-Borrmann eigenmodes propagate along the $z$ direction with different group velocities $v_{gz}^{(1)}$ and $v_{gz}^{(2)}$ in accordance with the pulse-splitting effect [red pulses in Fig. 6(b)]. We should note that instead

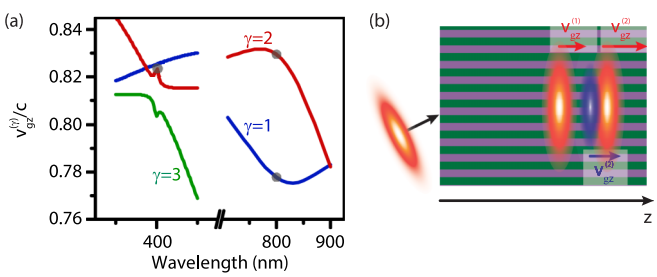


FIG. 6. (a) Spectral dependencies of the group velocities of eigenmodes of the PhC at the angle of incidence $\theta = 26.2^\circ$, which is the Bragg angle for $\lambda = 800$ nm. Dots indicate group velocities modes in the E-nonlinear process. (b) Sketch of the SHG in the PhC at the pulse splitting effect.

of the ordinary refraction, the fundamental light moves along the PhC's layers [Fig. 6(b)] that stems from the fact that the Poynting vector of a Bloch mode is orthogonal to its isofrequency curve and thus it is oriented along $z$ axis under the Bragg diffraction, when $k_x = h/2$ [Fig. 5(b)]. The calculated spectral dependencies of $v_{gz}^{(\gamma)}$ for the $p$-polarized eigenmodes are shown in Fig. 6(a). Valuable group velocities for $\lambda = 800$ and 400 nm are indicated by dots. Temporal delay between two fundamental pulses measured in the experiment for $L = 500$ $\mu$m [Fig. 3(b)] is in good agreement with the predicted value of $L|1/v_{gz}^{(1)} - 1/v_{gz}^{(2)}| = 133$ fs. In the considered phase-matched nonlinear process, cross-interaction of the two fundamental eigenmodes produces the source of the SH field in the region of spatial overlap of the fundamental pulses. This overlap decreases with the pulses propagation time thus resulting in the decrease of the nonlinear polarization. Nonmonotonic dependence of $\eta$ observed in the experiment is the result of the competition of the decrease of the fundamental pulse amplitude and increase of the overlap at the pulse widening.

To obtain the dependence $\eta(\tau)$ more formally, we solve the wave equation in slowly varying envelope approximation for the SH pulse envelope $A_{2\omega}^{(2)}(z,t)$:

$$\frac{\partial A_{2\omega}^{(2)}(z,t)}{\partial z} + \frac{1}{v_{gz,2\omega}^{(2)}}\frac{\partial A_{2\omega}^{(2)}(z,t)}{\partial t} = \frac{2\pi i(2\omega)^2}{k_{2\omega}c^2}P_{NL}(z,t)\exp(i\Delta k z), \quad (1)$$

where $k_{2\omega} = 2\omega/c$, $\Delta k = q_z^{(1)}(\omega) + q_z^{(2)}(\omega) - q_z^{(2)}(2\omega)$ is the phase-mismatch, $v_{gz,2\omega}^{(2)}$ is the group velocity of eigenmode $\gamma = 2$ at SH frequency.

$$P_{NL}(z,t) = \chi_{eff}^{(2)}A_\omega^{(1)}(z,t)A_\omega^{(2)}(z,t) \quad (2)$$

is the nonlinear polarization resulted from the overlap of two fundamental pulses with Gaussian envelopes

$$A_\omega^{(\gamma)}(z,t) = \frac{1}{\sqrt{\tau}}\exp\left(\frac{-(z/v_{gz,\omega}^{(\gamma)} - t)^2}{(\tau/2)^2}\frac{ln2}{2}\right), \ \gamma = 1,2. \quad (3)$$

The effective nonlinear susceptibility $\chi_{eff}^{(2)}$ depends on the spatial overlap of the SH eigenmode $\gamma = 2$ and the product of the fundamental eigenmodes $\gamma = 1, 2$ in the PhC's unit cell [47]. We applied Eq. (1) to describe the evolution of the SH pulse formed by the single SH eigenmode $\gamma = 2$ excited in the phase-matched process, i.e., for $\Delta k = 0$. We emphasize that two nonlinear polarization terms in Eq. (1) responsible for the self-interaction of the fundamental eigenmodes and proportional to $A_\omega^{(1)}$ and $A_\omega^{(2)}$ squared are omitted. It is justified by a large phase mismatch leading to the coherence length only of about $L_c \approx 9$ $\mu$m for the SHG driven by these terms. We also note that the effect of the dispersive broadening of the fundamental pulses does not affect the SHG inside the PhC and it was neglected in the calculations. It stems from small length of the PhC ($L$) compared to the dispersion length $L_d$ calculated from dispersion law of light in the PhC. For 60 fs laser pulses, it was estimated as $L_d^{(1)} \approx 7.5$ mm and $L_d^{(2)} \approx 3$ mm for fundamental eigenmodes with $\gamma = 1$ and

$\gamma = 2$, respectively, that is many times smaller $L$ and thus pulse spreading could be neglected.

The energy of the SH pulse is given by

$$\mathcal{E}_{2\omega} = \int \left|A^{(2)}_{2\omega}(L,t)\right|^2 dt. \quad (4)$$

Then $\eta$ is determined as the ratio of the SH pulse energy to the squared fundamental pulse energy: $\eta = \mathcal{E}_{2\omega}/{\mathcal{E}_\omega}^2$, that is equivalent to $\eta$ used in the experiment. Calculated dependencies $\eta(\tau)$ shown by solid curves in Fig. 4(b) for different values of the PhC length $L$ agree qualitatively with the experimental ones demonstrating the growth for short incident pulses, the decrease for stretched pulses and shift of the maximum to higher $\tau$ with the increase of $L$. The obtained dependencies reveal a linear growth originating from the increase of the PhC region where fundamental pulses are well spatially overlapped and then a decrease, which is inversely proportional to $\tau$, caused by reducing of the peak intensity of the pump pulses [Fig. 4(b)].

To reveal accurately the effects of finite spatial spectrum of pulses, angular dependence of propagation constants, group velocity dispersion in the dependence of the SHG in the PhC on the pulse duration, we applied the finite-difference time-domain (FDTD) method. For FDTD simulation, we developed the nonlinear FDTD code by modification of the open-source MEEP package [48]. Calculations were performed in the undepleted pump approximation, running in parallel the two simulations for the fundamental and the SH radiation. The light source in the SH simulation was the vectorial nonlinear polarization updated at every time step of the modeling on the basis of (i) the fundamental field determined in the previous time step, and (ii) specified spatial distribution of the second-order nonlinear susceptibility tensor. Similar approach was used successfully for the prediction of SHG in photonic crystal waveguides [49,50].

In numerical investigations, we considered 1D PhC similar to the experimental one with the length of $L = 250$ $\mu$m and the layer thicknesses of $d_1$ and $d_2$. We took into account the dispersion of the refractive indices of the PhC layers by setting different values of the refractive index of PhC's materials in simulation for the fundamental and SH wavelengths, i.e., we neglected the intrapulse dispersion. Assigned values of the refractive indices of PhC layers equal to $n_1$ and $n_2$ corresponded to the experimental ones described in Sec. II.

Special attention was paid to create Yee's mesh for accurate SHG modeling. We chose the spatial step $\Delta_{x,z}$ of the Yee's mesh to be sufficiently small to alleviate numerical dispersion inherent to the FDTD method [51]. Discretization of the Maxwell's equations in the FDTD algorithm leads to deviation of propagation constants of light in simulation from exact ones intrinsic to optical materials. We assert that in our two-step FDTD modeling of SHG, numerical dispersion leads to finite coherence length $L_c = \pi/\Delta k$ even when the phase-matched SHG is simulated, which may introduce a dramatic error in the SHG conversion efficiency for long structures as we consider. To cure this issue, we chose $\Delta_{x,z} = 4$ nm in such a way to give the coherence length $L_c = 4L$ that assures 3% simulation error in the nonlinear field amplitude. Calculations were performed on the supercomputer of Lomonosov Moscow State University.

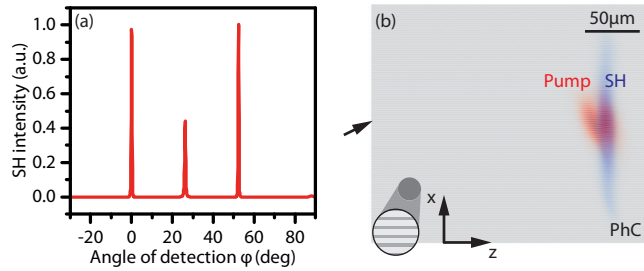


FIG. 7. (a) SH indicatrix calculated by nonlinear FDTD. (b) Calculated spatial distribution of light intensity of fundamental (red color) and SH (blue color) radiation. Shaded region is the PhC, the inset is enlarged view. Light propagates from left to right.

To simulate the pulse-splitting effect in SHG for $p$-polarization of light, we restrict ourselves by consideration of particular second-order nonlinear susceptibility tensor $\hat{\chi}^{(2)}$ with nonzero components of $\chi^{(2)}_{ijk} = 1$ for $i \neq y$ and attributed to the whole PhC. We note that the usage of actual values of $\hat{\chi}^{(2)}$ components of the experimental structure are not needed to simulate this effect as just the nonlinear polarization is required to excite the SH Bloch mode. Indeed, the choice of specific $\hat{\chi}^{(2)}$ just effects the effective nonlinear susceptibility $\hat{\chi}^{(2)}_{\text{eff}}$ determined by spatial overlap of the particular Bloch eigenmodes participating in the phase-matched SHG [47], remaining the underlying physics the same. So applied simplified tensor $\hat{\chi}^{(2)}$ is enough to simulate the effect. The latter condition $i \neq y$ guarantees the consideration of the phase-matched generation for the $p$-polarized SH light.

In simulation of the SHG in the PhC, the femtosecond $p$-polarized fundamental pulse with the waist size of 40 $\mu$m, central wavelength of 800 nm was incident at the Bragg angle of $\theta = 26.2^\circ$ onto the PhC's facet. The duration of the laser pulse $\tau$ was varied in the range of 30–150 fs.

Figure 7(b) shows the calculated spatial distributions of the intensity of the fundamental (red) and generated SH (blue) pulses propagating along the Oz axis from left to the right for the incident pump pulse duration of $\tau = 40$ fs. As seen, the propagation of the fundamental pulse causes it to split into a pair of pulses distanced by 12 $\mu$m after passing 200 $\mu$m in the PhC, thus demonstrating the pulse-splitting effect. In turn, the SH radiation is grouped in a single pulse, which propagates almost together with the fastest pump pulse. It is in agreement with the calculated values of the group velocities of eigenmodes at the pump and SH wavelengths shown by dots in Fig. 6(a). Curiously, the SH radiation has a wider lateral spatial distribution (along Ox direction) than the fundamental ones [Fig. 7(b)]. We address this effect to a strong divergence of the SH beam resulted from the interplay of (i) finite width of the lateral spatial spectrum of the nonlinear polarization and (ii) a strong dependence of the direction of the Poynting vector for the eigenmode $\gamma = 2$ at the SH frequency on $k_x$. The latter takes place due to the presence of the degeneracy point with the linear dispersion in the photonic band structure in the vicinity of the SH frequency. Indeed, in the considered case of the phase-matching condition E, at the SH frequency, the propagation constants $q_z^{(2)}$ and $q_z^{(3)}$ are almost the same [see red and green dashed curves in Fig. 5(a)] and the SH isofrequency curves $\gamma = 2,\ 3$ are approaching each other [see

red and greed dashed curves in Fig. 5(b)]. This results in a crucial change of the Poynting vector direction of the eigenmode $\gamma = 2$, which is orthogonal to the isofrequency curve, at detuning of $k_x$ from $h$. This explains that diffraction spreading of the SH pulse is much stronger than for the fundamental ones.

Next, the calculated radiation pattern of the outgoing SH light exhibits three pronounced diffraction maxima [Fig. 7(a)] that are in agreement with the experimental indicatrix [Fig. 2(a)]. The appearance of the strong central maximum at $\varphi = 26.2^\circ$ is a peculiar feature that is opposite to previous observations of SHG in similar PhCs in the Laue geometry of diffraction [35] and speculations based on self-action of light in Ref. [36]. We assert that in considered case it stems from the phase-matched excitation of the SH eigenmode $\gamma = 2$, which possesses symmetric spatial field distribution in a PhC's unit cell with respect to center one of the layers. The amplitudes of spatial Fourier components of $E_x$ field of this eigenmode are shown in Fig. 2(b) by red curves. As seen, this eigenmode has nonzero Fourier component corresponding to $k_x = 0$, resulting in the appearance of discussed SH diffraction maximum along Oz axis when this eigenmode approaches the output PhC's facet.

Finally, the calculated dependence of $\eta(\tau)$ shown by dots in Fig. 4(b) is in a good agreement with the results of the experiment for the PhC with $L = 250$ $\mu$m exhibiting the maximum of normalized SH power at incident laser pulse duration of $\tau = 60$ fs. The FDTD results agree well with the slowly varying envelope approach indicating that the group velocity dispersion, diffraction spreading are not crucial in the effect of SHG under the pump pulse splitting in the PhC and simplified model of slow varying envelope is adequate to describe the considered dynamical nonlinear phenomenon.

## IV. CONCLUSION

Summing up, in this work we studied experimentally and numerically the phase-matched SHG in 1D PhCs in the Laue scheme of diffraction supporting the effect of the diffraction-induced splitting of the fundamental femtosecond laser pulse, i.e., splitting of a single incident pulse to pair pulses in a PhC. We experimentally showed the phase-matched SHG involving two fundamental eigenmodes and a single one at the SH frequency that was achieved by tuning the thicknesses of the PhC' layers. We demonstrated that in this particular case the SHG is strongly affected by the pulse-splitting effect and dynamics of fundamental field inside the PhC is primary important. We revealed experimentally and numerically that dependence of the second harmonic power on the duration of the incident femtosecond laser pulse is significantly nonmonotonic. The increase of the laser pulse duration while maintaining the incident pulse energy leads to an increase of the nonlinear signal for short laser pulses and a decrease for long pulses. It allows one to maximize the SH conversion efficiency by tuning the laser pulse duration. We provided a theoretical insight into the physical mechanisms of the observed phenomenon, asserting a competition of the two factors at the pulse stretching and the presence of the pulse-splitting effect: (i) increase of the spatial overlap of the fundamental pulses and (ii) decrease of their pick intensity. Using the two different approaches of 1D slow-varying envelope method and the exact 2D nonlinear FDTD simulation, we confirmed the experimental results.

We believe that the revealed dynamical effect in the frequency light conversion can be useful in the nonlinear optics of multimode PhC fibers as well [39,40]. In this case, the nonlinear interaction of the laser pulses associated with different guided eigenmodes could be affected by the discussed effects. Our findings open a way to maximize the nonlinear signal yield in these systems. Moreover, PhC fibers have wide capabilities in tuning the group velocities and support the zero-dispersion regime giving a possibility to treat even shorter optical pulses. We suppose that the observed phenomena can be extended to the high harmonic generation in high-power laser applications. Recently, plasma PhCs formed by periodically modulated in space electron density were proposed, offering a versatile control of the high-intensity femtosecond laser pulses with the overcome of the damage threshold of solid-state structures [52,53]. We believe that obtained results of the harmonic generation in the Laue diffraction scheme in 1D PhCs can be applied to these physical systems opening a way for harmonic generation in plasma PhCs.

## ACKNOWLEDGMENTS

The authors are thankful to B. I. Mantsyzov for fruitful and encouraging discussions. The research is carried out using the equipment of the shared research facilities of HPC computing resources at Lomonosov Moscow State University. This work was supported by Russian Science Foundation Grant No. 19-72-00118.

[1] R. W. Boyd, Nonlinear Optics (Academic Press, 2020).
[2] M. Kauranen and A. V. Zayats, Nat. Photonics **6**, 737 (2012).
[3] G. Li, S. Zhang, and T. Zentgraf, Nat. Rev. Mater. **2**, 1 (2017).
[4] B. Sain, C. Meier, and T. Zentgraf, Adv. Photonics **1**, 1 (2019).
[5] J. Butet, P.-F. Brevet, and O. J. Martin, ACS Nano **9**, 10545 (2015).
[6] G. Bachelier, J. Butet, I. Russier-Antoine, C. Jonin, E. Benichou, and P.-F. Brevet, Phys. Rev. B **82**, 235403 (2010).
[7] K. Thyagarajan, S. Rivier, A. Lovera, and O. J. Martin, Opt. Express **20**, 12860 (2012).
[8] A. L. Chekhov, I. Razdolski, A. Kirilyuk, T. Rasing, A. I. Stognij, and T. V. Murzina, Phys. Rev. B **93**, 161405(R) (2016).
[9] V. B. Novikov, A. A. Nasonov, A. I. Maydykovskiy, and T. V. Murzina, JETP Lett. **108**, 296 (2018).
[10] F. Timpu, A. Sergeyev, N. R. Hendricks, and R. Grange, ACS Photonics **4**, 76 (2016).
[11] Y. Kivshar and A. Miroshnichenko, Opt. Photon. News **28**, 24 (2017).
[12] E. V. Melik-Gaykazyan, M. R. Shcherbakov, A. S. Shorokhov, I. Staude, I. Brener, D. N. Neshev, Y. S. Kivshar, and A. A. Fedyanin, Philos. Trans. R. Soc. A **375**, 20160281 (2017).

[13] K. Frizyuk, I. Volkovskaya, D. Smirnova, A. Poddubny, and M. Petrov, Phys. Rev. B **99**, 075425 (2019).

[14] K. Koshelev, Y. Tang, K. Li, D.-Y. Choi, G. Li, and Y. Kivshar, ACS Photonics **6**, 1639 (2019).

[15] J. A. Armstrong, N. Bloembergen, J. Ducuing, and P. S. Pershan, Phys. Rev. **127**, 1918 (1962).

[16] A. Chowdhury, H. M. Ng, M. Bhardwaj, and N. G. Weimann, Appl. Phys. Lett. **83**, 1077 (2003).

[17] I. V. Shutov, I. A. Ozheredov, A. V. Shumitski, and A. S. Chirkin, Opt. Spectrosc. **105**, 79 (2008).

[18] J. Van der Ziel, Appl. Phys. Lett. **26**, 60 (1975).

[19] A. Fiore, S. Janz, L. Delobel, P. van der Meer, P. Bravetti, V. Berger, E. Rosencher, and J. Nagle, Appl. Phys. Lett. **72**, 2942 (1998).

[20] N. Bloembergen and A. Sievers, Appl. Phys. Lett. **17**, 483 (1970).

[21] J. P. van der Ziel and M. Ilegems, Appl. Phys. Lett. **28**, 437 (1976).

[22] A. Yariv and P. Yeh, J. Opt. Soc. Am. **67**, 438 (1977).

[23] M. Scalora, M. J. Bloemer, A. S. Manka, J. P. Dowling, C. M. Bowden, R. Viswanathan, and J. W. Haus, Phys. Rev. A **56**, 3166 (1997).

[24] A. V. Balakin, V. A. Bushuev, B. I. Mantsyzov, I. A. Ozheredov, E. V. Petrov, A. P. Shkurinov, P. Masselin, and G. Mouret, Phys. Rev. E **63**, 046609 (2001).

[25] Y. Dumeige, I. Sagnes, P. Monnier, P. Vidakovic, I. Abram, C. Mériadec, and A. Levenson, Phys. Rev. Lett. **89**, 043901 (2002).

[26] A. Maydykovskiy, V. Novikov, S. Svyakhovskiy, and T. Murzina, Crystals **4**, 427 (2014).

[27] V. B. Novikov, S. E. Svyakhovskiy, A. I. Maydykovskiy, T. V. Murzina, and B. I. Mantsyzov, J. Appl. Phys. **118**, 193101 (2015).

[28] S. E. Svyakhovskiy, A. I. Maydykovskiy, V. B. Novikov, V. O. Kompanets, A. A. Skorynin, V. A. Bushuev, S. V. Chekalin, T. V. Murzina, and B. I. Mantsyzov, J. Russ. Laser Res. **36**, 588 (2015).

[29] V. B. Novikov and T. V. Murzina, Opt. Lett. **42**, 1389 (2017).

[30] V. B. Novikov and T. V. Murzina, Phys. Rev. B **99**, 245403 (2019).

[31] B. Mantsyzov, Opt. Commun. **189**, 275 (2001).

[32] V. A. Bushuev, L. V. Dergacheva, and B. I. Mantsyzov, Phys. Rev. A **95**, 033843 (2017).

[33] D. M. Tsvetkov, V. A. Bushuev, and B. I. Mantsyzov, Phys. Rev. A **99**, 023846 (2019).

[34] D. M. Tsvetkov, V. A. Bushuev, V. V. Konotop, and B. I. Mantsyzov, Phys. Rev. A **98**, 053844 (2018).

[35] V. B. Novikov, A. I. Maydykovskiy, B. I. Mantsyzov, and T. V. Murzina, Phys. Rev. B **93**, 235420 (2016).

[36] D. A. Kopylov, S. E. Svyakhovskiy, L. V. Dergacheva, V. A. Bushuev, B. I. Mantsyzov, and T. V. Murzina, Phys. Rev. A **93**, 053840 (2016).

[37] B. Corcoran, C. Monat, C. Grillet, D. J. Moss, B. J. Eggleton, T. P. White, L. O'Faolain, and T. F. Krauss, Nat. Photonics **3**, 206 (2009).

[38] H. Tu, Z. Jiang, D. L. Marks, and S. A. Boppart, Appl. Phys. Lett. **94**, 101109 (2009).

[39] S. Signorini, M. Mancinelli, M. Borghi, M. Bernard, M. Ghulinyan, G. Pucker, and L. Pavesi, Photon. Res. **6**, 805 (2018).

[40] J. Demas, L. Rishøj, X. Liu, G. Prabhakar, and S. Ramachandran, Photon. Res. **7**, 1 (2019).

[41] H. Pourbeyram and A. Mafi, Phys. Rev. A **94**, 023815 (2016).

[42] M. Ziemienczuk, A. M. Walser, A. Abdolvand, and P. S. J. Russell, J. Opt. Soc. Am. B **29**, 1563 (2012).

[43] J. Yuan, Z. Kang, F. Li, G. Zhou, X. Sang, Q. Wu, B. Yan, X. Zhou, K. Zhong, L. Wang, K. Wang, C. Yu, C. Lu, H. Y. Tam, and P. K. A. Wai, Opt. Lett. **42**, 1644 (2017).

[44] S. E. Svyakhovskiy, A. A. Skorynin, V. A. Bushuev, S. V. Chekalin, V. O. Kompanets, A. I. Maydykovskiy, T. V. Murzina, V. B. Novikov, and B. I. Mantsyzov, J. Opt. Soc. Am. B **30**, 1261 (2013).

[45] M. J. Sailor, *Porous Silicon in Practice: Preparation, Characterization and Applications* (John Wiley & Sons, 2012).

[46] S. E. Svyakhovskiy, A. I. Maydykovsky, and T. V. Murzina, J. Appl. Phys. **112**, 013106 (2012).

[47] K. Sakoda and K. Ohtaka, Phys. Rev. B **54**, 5742 (1996).

[48] A. F. Oskooi, D. Roundy, M. Ibanescu, P. Bermel, J. Joannopoulos, and S. G. Johnson, Comput. Phys. Commun. **181**, 687 (2010).

[49] F. Raineri, Y. Dumeige, A. Levenson, and X. Letartre, Electron. Lett. **38**, 1704 (2002).

[50] Y. Dumeige, F. Raineri, A. Levenson, and X. Letartre, Phys. Rev. E **68**, 066617 (2003).

[51] J. B. Schneider, Understanding the Finite-Difference Time-Domain Method (2010).

[52] G. Lehmann and K. H. Spatschek, Phys. Rev. Lett. **116**, 225002 (2016).

[53] G. Lehmann and K. H. Spatschek, Phys. Plasmas **24**, 056701 (2017).